EUROPEAN ORGANIZATION FOR NUCLEAR RESEARCH

CERN-EP/98-59
5.5.1998

Meson-exchange enhancement in first-forbidden beta transitions. The case of ^{50}K and ^{38}Ca

P. Baumann, M. Bounajma, F. Didierjean* A. Huck, A. Knipper,
M. Ramdhane** and G. Walter

Institut de Recherches Subatomiques, Université Louis Pasteur, 67037 Strasbourg, France and the ISOLDE Collaboration

G. Marguier

Institut de Physique Nucléaire, Université Claude Bernard, 69622 Villeurbanne, France and the ISOLDE Collaboration

C. Richard-Serre

IN2P3 and CERN, CH - 1211 Genève 23, Switzerland

B.A. Brown

NSCL and Department of Physics and Astronomy, Michigan State University, East Lansing, Michigan 48824, USA

Abstract

The β decay of ^{50}K and ^{38}Ca have been investigated with the main motive of determining more accurately the first-forbidden β branches, in particular the rank-zero, $\Delta J = 0$, β transitions. ^{50}K and ^{38}Ca have been produced by fragmentation of U and Ti targets respectively, with a 1 GeV proton beam and subsequent on-line mass separation. For ^{50}K, gamma-ray spectroscopy, as well as delayed neutron spectroscopy by time of flight, were carried out to obtain a detailed decay scheme to 20 (bound and unbound) levels in ^{50}Ca. The level structure of ^{50}Ca can be compared to recent calculations which incorporate 1p1h excitations from the $f_{7/2}$ shell. The first-forbidden β^- transition $^{50}\mathrm{K}(0^-) \rightarrow {}^{50}\mathrm{Ca}(0^+)$ g.s. has been evaluated for the first time by a direct measurement of β and γ activities. Its importance $(61.0 \pm 7.4\,\%)$ is interpreted as an effect of the meson-exchange current (MEC) leading to an enhancement factor of 62(5) % in comparison with the value predicted by shell-model calculations using the impulse approximation. For the $^{38}\mathrm{Ca} \rightarrow {}^{38}\mathrm{K}$ decay, chemical selective production was obtained through separation of the molecular ion CaF^+ without contamination by isobars. In these conditions, the measurement of very weak beta branches, at a level of 10^{-3} per 100 decays, could be made and a limit, at the 2σ confidence level, has been obtained for the $0^+ \rightarrow 0^-$ branch to the level at $E_x = 2993$ keV ($I_\beta < 0.0046\,\%$).

Implications of these results on the general trend of meson-exchange enhancements of first-forbidden transitions within the framework of the spherical shell model are discussed.

(IS308)

(Submitted to Phys. Rev. C)

---

* present address : Eurisys, Strasbourg-Lingolsheim, France

** present address : University of Constantine, Algeria

PACS : 23.40.Hc
27.40.+z 23.20.Lv 21.60.Cs

1 INTRODUCTION

The enhancement of the β decay rate by mesonic-exchange currents (MEC) was predicted by calculations [1, 2] and explained as a contribution of the meson exchange, mostly pions, to the time-like component of the weak-axial current. The importance of this enhancement, with respect to the impulse approximation, was predicted to be of the order of 50 % in a wide range of nuclear masses and also to be insensitive to nuclear structure [3, 4]. These predictions have been found in good agreement with the experimental results and the enhancement factor over the impulse approximation, $\epsilon_{\rm MEC} \approx 1.64$ has been deduced in the A=16 and A=96 region [5, 6, 7]. Studies in the lead region have established a larger factor $\epsilon_{\rm MEC}$ (2.01 ± 0.05) [8] which exceeds the value caused by pion exchange alone. Different theoretical explanations [9, 10] have been proposed to explain this enhancement and precise experimental determinations of $\Delta J = 0$ first-forbidden transitions are still clearly of high interest.

In the cases previously studied near ^{16}O, ^{96}Zr and ^{208}Pb, the main component of the first-forbidden decay is given by a ν $s_{1/2} \rightarrow \pi$ $p_{1/2}$ transition. We report here on measurement of the $0^- \rightarrow 0^+$ and $0^+ \rightarrow 0^-$ pseudoscalar decays in ^{50}K and ^{38}Ca respectively, where the dominant component arises from a ν $p_{3/2} \rightarrow \pi$ $d_{3/2}$ transition. We wanted to verify that the enhancement factor was insensitive to the nature of the valence shell. In the first-forbidden β decay only rank-zero matrix elements are present: the time-like component $M_0^T = \int \gamma_5$ and the space-like component $M_0^S = \int \bar{\sigma} \cdot \bar{r}$, related to the γ_5, σ and r operators.

The experimental value of the rank-zero matrix elements is obtained, with a very good approximation [11] from the transition strength of the first-forbidden decay:

$$B_1^0 = \left[M_1^0\right]^2 = 9195.10^5 / f_0\, t \ \ \mathrm{fm}^2 \tag{1}$$

with t, the partial half-life of the beta transition and f_0 the phase-space factor.

The calculated matrix element is expressed as:

$$M_1^0 = \epsilon_{\rm MEC}\, M_0^T + a_s M_0^S \ \ \mathrm{fm} \tag{2}$$

where the constant $a_s = a_s(Z, W_0, r)$, is a kinematical factor [11].

The enhancement factor over the impulse approximation, $\epsilon_{\rm MEC}$, is obtained from the comparison of equations (1) and (2).

A previous study of the decay scheme of ^{50}K [12] suggested a strong ground state feeding of ^{50}Ca (≈ 60 %) which was inferred from unobserved activity in neutron and gamma measurements. The resulting log ft value (log f_0t $= 5.89 \pm 0.09$) could only be interpreted as a $0^- \rightarrow 0^+$ transition with a strong enhancement. A shell-model calculation of this transition, with an evaluation of core-polarization effects, was made by Warburton [13]. Comparison to experiment indicates the need for a large mesonic enhancement for the time-like component of the weak- axial current, in agreement with the general trend in $\Delta J = 0$ first-forbidden decays in A = 16 to 96 nuclei. Nevertheless, a direct and more precise measurement of the β feeding to ^{50}Ca g.s. was required to confirm these first evaluations [14].

We report here on the direct observation of this branch by simultaneous beta and gamma measurements. These determinations, as well as neutron spectroscopy measurements improved significantly the knowledge of the decay modes of ^{50}K and of the level structure of ^{50}Ca. They provide also valuable tests for calculations with an effective interaction away from the stability line.

In the case of the ^{38}Ca decay, the work of Wilson et al. [15] using the activity induced by the (^{3}He,n) reaction on a ^{36}Ar target gave neither value nor limit for the transition ^{38}Ca(0^+, g.s.) $\rightarrow$ ^{38}K(0^-, E_x = 2993 keV). A weak intensity for this branch ($I_\beta = 0.03$ %) has been predicted by Warburton et al. [11] using a current value for the enhancement factor ($\epsilon_{\rm MEC} = 1.64$). A significant improvement of the experimental techniques in on-line mass spectrometry allowed us to measure in detail the ^{38}Ca decay and to search for weak branches. In this paper we discuss the upper limit we find for the first-forbidden transition. Our results related to the Gamow-Teller strength have been reported separately [16].

2 EXPERIMENTAL PROCEDURES

2.1 Production of the isotopes

All the experiments were performed at CERN with the 1-GeV pulsed proton beam from the PS-Booster and with the on-line mass separator ISOLDE.

Potassium isotopes were produced by bombarding an UC_2 target (50 g/cm^2). The atoms were ionized through surface ionisation and mass separated in the ISOLDE magnet. The proton pulses had 2.4 μs width and a spacing of an integer multiple of 1.2 s. The resulting average beam intensity was 2 μA. The opening of the ISOLDE beam gate was delayed 10 ms with respect to the proton pulse and maintained for different duration depending on the measurements. The identification of the observed activities was made difficult for two reasons: the presence of short half-life daughter activities (sketched on Fig. 1) and the simultaneous production of the isobars: ^{50}K (472 ms), ^{50}Ca (13.9 s), ^{50}Sc (1.71 min), ^{50m}Sc (0.35 s) produced and ionized concurrently with different yields. The yield for ^{50}K was about 5.10^4 at/μC. The ion beam was directed onto an aluminized-mylar tape. A fraction of the daughter activities was periodically removed by driving the tape.

Calcium isotopes were produced by bombarding a Ti rod target (93 g/cm^2) with the proton beam. The beam gate was delayed 10 ms and had a 500 ms opening time. The experimental difficulty was the search of a weak line in the ^{38}Ca decay ($T_{1/2}$ = 440 ms), in presence of the strong activity of the isobars ^{38}K ($T_{1/2}$ = 7.64 min.) and ^{38m}K ($T_{1/2}$ = 924 ms). These isobars, closer to stability, are favored by the production cross section, the ionization efficiency and the half-life. Therefore, the production yield for ^{38}K was higher by a factor 10^4 to the ^{38}Ca one. As detailed in reference [16], the required selectivity for Ca versus K was obtained by using molecular ions CaF^+ [17] obtained by fluoration of the reaction products inside the target-ion source assembly. Molecular ions of $^{38}Ca^{19}F^+$ were selected with the isotope separator magnet adjusted for A = 57. The CaF^+ ion beam was directed onto the collecting point of the tape-transport system.

2.2 Measurement of $\beta - \gamma$ coincidences

In the ^{50}K experiment, the β emission was detected in thin cylindrical plastic scintillators, surrounding the tape in a near 4π geometry in two different positions: at the collecting point for β-delayed neutron coincidences and at a remote position, 30 cm above the collecting point, for low background decay measurements. At this place, the β emission was registered in a multiscaling mode, allowing to determine the contribution of each isobar.

The γ spectra were recorded in two large (70 %) Ge detectors. Relative γ-ray efficiencies were measured with ^{56}Co and ^{152}Eu sources. The relative efficiency of the β and γ counters was obtained by measuring in the same conditions, the β activity and the corresponding γ intensity of the well-known ^{26}Na radioisotope [18]. From the beta intensity deduced from the multiscaling spectrum (Fig. 2) and the gamma simultaneous measurement of the 1808 keV line (^{26}Mg), we deduced the efficiency ratio: $\epsilon_\beta/\epsilon_\gamma$ for E_γ = 1808 keV. The decay pattern of the β-multiscaling (Fig. 1) is also a test of the purity of the mass-separated sources. The γ spectra were recorded in singles, in coincidences ($\beta - \gamma$ and $\beta - \gamma - \gamma - t$) and in multispectrum mode. The intensity determination of β branches in the ^{50}K decay was made via simultaneous β and γ measurements.

In the ^{38}Ca experiment, the setup was devised to optimize the ^{38}Ca beta-delayed γ detection over background for the observation of very weak gamma lines. In addition to the thin cylindrical plastic detector, surrounding the tape in a near 4π geometry, two thin flat (2 mm thick) plastic scintillators were placed in front of each Ge detector and operated as veto counters to avoid the simultaneous detection of positrons and gamma rays in the same counter. No contaminants were identified in the CaF^+ molecular beam which, contrary to the potassium case, is free from isobaric contribution.

2.3 Measurement of β-delayed neutrons

The intensities of the transitions to the neutron-emitting states in ^{50}Ca were obtained by neutron time-of-flight measurements using two types of detectors:

- for the low energy neutrons, 12 small plastic (NE102A) scintillators (1 cm thick, diameter 10 cm), associated each to two photo-tubes XP 2020 operated in coincidence, have been used with a flight path of 75 cm. The threshold for the fast triggers was below the one photoelectron level and the resulting energy threshold was about 20 keV. For the design of this device [19] we took into account the developments made at Oak Ridge by Hill and al. [20] for neutron diffusion studies at low energy. In the present experiment, the array of detectors (Fig. 3) was used as a unique counter by mixing the signals delivered by each coincidence circuit

- for the upper part of the neutron spectrum, complementary information was obtained with a large (2880 cm^2) curved plastic counter [21, 22], which is thicker (1.25 cm) and is used with a longer fligth path (100 cm).

3 RESULTS

3.1 The ^{50}K β decay

3.1.1 Determination of the intensity of the β branches to bound states in ^{50}Ca

The ^{50}K β emission was registered in a multiscaling mode and reveals the presence of different components (Fig. 4) corresponding to the A = 50 isobars and the daughters activities. The curve was analysed allowing various contributions of each emitter (^{50}K decay, ^{50}Ca produced directely by the source and by ^{50}K decay, ^{50}Sc, ^{50m}Sc produced directely and by ^{50}Ca decay). All decay modes (Fig. 1) were taken into account in the calculated decay curve. The best fit with the experimental curve was obtained for a relative intensity, I, for the different isobars : $I_1 = 1$ (^{50}K, 472 ms), $I_2 = 0.24$ (^{50}Ca, 13.9 s), $I_3 = 0.13$ (^{50}Sc, 1.71 min), $I_4 = 0.16$ (^{50m}Sc, 0.35 s). From this analysis we deduce the direct production of ^{50}Ca (3.4 10^3 at/μC), ^{50}Sc (5.1 10^4 at/μC) and ^{50m}Sc (11.6 10^4 at/μc).

If N_c is the total number of ^{50}K atoms collected on the tape and moved to the measuring station, the number of ^{50}K disintegrations, N_β, in the measuring time t_m, is:

$$N_\beta = (N_c \epsilon_\beta / \lambda_1)(\exp -\lambda_1 t_t)(1 - \exp -\lambda_1 t_m) \tag{3}$$

with $\lambda_1 = 0.693/T = 1.468\ s^{-1}$, T: ^{50}K half-life, t_t the transport duration and ϵ_β the β detector efficiency.

In the thin scintillator, the β energy loss, and then ϵ_β, are independent of the energy with a good approximation.

The number of ^{50}K disintegration, N_γ, registered via the main γ-delayed transition in ^{50}Ca (1027 keV) is:

$$N_\gamma = (N_c \epsilon_{\gamma(1027\,keV)} X / \lambda_1)(\exp -\lambda_1 t_t)(1 - \exp -\lambda_1 t_m) \tag{4}$$

with $\epsilon_{\gamma(1027\,keV)}$ the γ detector efficiency at 1027 keV and X.100, the number of 1027 keV γ transitions for 100 ^{50}K disintegrations.

From (3) and (4) we obtain the intensity of the 1027 keV γ line:

$$X = \epsilon_\beta / \epsilon_{\gamma(1027\,keV)} (N_\gamma / N_\beta) \tag{5}$$

We have identified eight γ transitions in ^{50}Ca consecutive to the ^{50}K beta decay. Their energy and intensity are listed in **Table I**. The $\beta - \gamma - \gamma -$ t coincidence analysis leads to an extended level scheme for the low-lying levels in ^{50}Ca with two new levels at 3532 and 4476 keV. As an example the $\beta - \gamma$ spectrum

corresponding to a 1027 keV gate, is shown in Fig. 5. It reveals a doublet, 2498 keV (3009 single escape) and 2505 keV deexciting the new level at 3532 keV. The γ-ray branching ratios in ^{50}Ca are listed in **Table II**. From these measurements we deduce the β intensities to the ^{50}Ca bound excited levels (**Table III**) taking into account the intensity of the 1027 keV γ line, the relative efficiency ratio $\epsilon_{\gamma(1808keV)}/\epsilon_{\gamma(1027keV)}$ and the γ intensity balance of the 1027 keV state. We have also reported in **Table III** the intensity of the beta branches to the neutron-unbound states which have been obtained from the neutron measurements discussed in the next section.

In the ^{50}K decay, the β total intensity to the neutron-unbound states in ^{50}Ca is known from previous measurements [23, 24] with a resulting weighted mean $P_n = 29 \pm 3\,\%$. The value $100 - P_n$ corresponds to the sum of the β_0 branch to the ground state and the β branches to the excited states in ^{50}Ca. By difference we obtain the β intensity to the ^{50}Ca ground state: $I_{\beta_0} = 61.0 \pm 7.4\,\%$.

3.1.2 Determination of the intensity of the β branches to unbound states in ^{50}Ca

The neutron spectrum, recorded with the multidetector device operated as a unique counter by mixing the signals given by the 12 coincidence circuits is given in Fig. 6. From this spectrum, we have obtained the relative intensity of the different peaks after correction with the neutron detection efficiency. This efficiency has been calculated between 20 keV and 5 MeV, taking into account the specifications of the scintillators and the position of the detector threshold. The resulting values are reported in **Table IV** and can be compared to previous measurements made by Ziegert [25] with ^{3}He neutron detectors. Results given by the two techniques are found in good agreement with a better resolution given by the gas counter at low energy but a much better efficiency at high energy with the organic scintillator. In **Table IV**, we have also reported the four values above 3.4 MeV measured with better accuracy in the large curved scintillator. It should be noted that the excitation energies reported in **Table IV** at high energy ($E_x \geq 9$ MeV) result from the observation of maxima in the neutron spectra and may correspond to several unresolved states strongly populated by beta decay. The resulting B(GT) value, which is discussed in the next section, is summed up in 500 keV intervals and is identical if the beta strength is distributed on one or several nearby states.

For the assignment of the neutron branches to transitions between levels of ^{50}Ca and ^{49}Ca, we have taken into account energy and intensity of gamma transitions in ^{49}Ca measured in this experiment and reported in **Table V**. After efficiency correction, the total intensity of the neutron branches attributed to the population of excited states in ^{49}Ca is in agreement with the total intensity of ^{49}Ca gamma lines, measured during the same time. We have also used the information given by previous n-γ measurements [26]. A comparison of **Table IV** and **Table V** reveals that the neutron feeding of the level at 3860 keV has only been observed in the γ spectrum but no indication has been found in n-γ coincidences allowing to assign the corresponding neutron branch. Nevertheless we have identified the γ transition observed at 3859.7(9) keV with the deexcitation of the level at 3861(2) keV ($3/2^-$) in ^{49}Ca, observed in (d,pγ) work [27].

3.1.3 Decay scheme of ^{50}K

The level scheme established on the basis of our measurements is shown in Fig. 7. Spin assignments for bound levels of ^{49}Ca are taken from the literature. ^{50}K low energy levels are dominated by the $(\pi d_{3/2})^{-1}(\nu p_{3/2})^1$ configuration which yields to the J^π values of 0^-, 1^-, 2^-, 3^-. The two states connected by the strong β_0 branch are necessarily of different parity. From systematics and theory of first-forbidden decays in A $\approx$ 40, Warburton [13] concluded that the intensity of the β_0 branch, as evaluated in the first studies of ^{50}K decay [28, 12], establishes the ^{50}K ground state as $J^\pi = 0^-$. This finding is corroborated by the first-forbidden unique character of the transition to the 2^+ state at 1027 keV for which we report $\log f_0 t = 6.95$ and $\log f_1 t = 9.59$. For ^{50}Ca bound levels at 3002, 3532, 4036, 4476 and 4886 keV, we tentatively assign the spin and parity values reported in Fig. 7 on the basis of $\log ft$ values and γ-rays branching ratios. For these levels, the β-decay rates limit ΔJ ($\Delta J \leq 2$) and positive parity is expected at low energy. As a strong radiative transition to the ground state has been observed, we eliminate $J^\pi = 0^+$ as possible

assignment. Two levels (3532 and 4476 keV) are reported for the first time. In fact, the level at 4476.0(7) keV could be identified to the 0^+ level observed previously in a (t,p) experiment at 4470(15) keV [14]. Taking into account $J^\pi = 0^-$ for ^{50}K g.s., the neutron unbound states in ^{50}Ca populated by fast Gamow-Teller transitions are restricted to $J^\pi = 1^-$.

As it can be seen in Fig. 7, beta branches are distributed in three classes, according the energy:

- at high excitation energy, allowed β transitions populate neutron-unbound states corresponding to particle-hole, negative parity, configurations
- at lower excitation energy, forbidden β transitions to positive-parity bound states amount to a small fraction (4-5%) of the β decay
- finally, for the ^{50}Ca g.s. feeding, we observe a first-forbidden enhanced transition of 61.0(7.4) % with $\log f_0 t = 5.89(6)$.

The negative-parity states of ^{49}Ca, populated by neutron emission should correspond to $\ell = 0$ and $\ell = 2$ transfers. The result of this part of our study is a detailed decay scheme with a much improved confidence in the β intensities leading to a significant comparison with theoretical estimates. In Fig. 7, we have also shown the low-energy level scheme of ^{50}Ca, obtained with the FPD6 two-body interaction [29] within the full fp shell configuration space. A one to one relation can be established between the low-lying natural parity levels involved in this work and the calculated ones. The 4^+ indicated at 4.83 MeV from the (t,p) experiments [14] is also consistent with the FPD6 calculation.

We have reported in Fig. 8 the experimental distribution of the Gamow-Teller transition strength with the values taken from **Table III**. It appears clearly that the GT strength is located above 8.5 MeV. Its determination could only be done by neutron spectroscopy.

If we now focus on the Ca-Ti-Cr isotopic anomalies found in certain meteoritic inclusions namely in the meteorite of Allende, the 6510 keV level in ^{50}Ca could play a role in the ^{50}Ti/^{48}Ti abundance [30]. To explain the abundance of ^{50}Ti produced by the ^{50}Ca β decay (Fig. 1) these authors put forward a resonance in the neutron-capture $^{49}\mathrm{Ca} + \mathrm{n}$ reaction corresponding to the 6510 keV state and decaying by E1 gamma transition to the ^{50}Ca, 0^+ g.s.. This state presents properties which could fulfil the hypothesis of Sandler et al. [30]:

- the state is close to the $^{49}\mathrm{Ca} + \mathrm{n}$ threshold and can be populated at the stellar temperature
- the spin and parity values $J^\pi = 1^-$ are compatible with the β decay ($\log ft = 6.27$)
- the resonance in the capture reaction implies a $l = 0$ wave, which has the greatest transmission factor at low neutron energy.

Unfortunately no radiative decay was observed for this state in our measurement. An upper limit for the γ emission can be evaluated by comparison with the intensity of the 1027 keV γ ray and expressed as photons per 100 decays of the parent isotope. We found $I_\gamma \leq 0.011$ %.

The neutron width ($\Gamma_n = 7.5$ keV) was deduced by Kratz [31] from an analysis of the 155 keV neutron peak corresponding to the deexcitation of the 6510 keV level. In our measurement, the β branch to the 6510 keV level amounts to 1.28 % and therefore the upper limit for the gamma width, Γ_γ is

$$\Gamma_\gamma \leq (0.011/1.28) \times 7.5\,\mathrm{keV}$$

$$\Gamma_\gamma \leq 64\,\mathrm{eV}$$

In Weisskopf units, this value ($\Gamma_\gamma \leq 0.25$ W.u.) corresponds to an upper limit for the E1 transitions experimentally observed [18]. Consequently, the radiative decay is not excluded by our measurement but its observation needs a more sensitive technique.

3.2 $\Delta J = 0$, First-forbidden transitions in the ^{38}Ca beta decay

With the improved experimental conditions of this work (purity of the ^{38}Ca beam and selectivity of the detection device), we have searched for the β branch corresponding to the ^{38}Ca, $0^+ \rightarrow {}^{38}$K, 0^-, E_x = 2993 keV transition, predicted with an intensity of 0.03 % [11]. The $J^\pi = 0^-$ character of the 2.99 MeV level has been firmly established by Rickel et al. [33] and the radiative decay takes place through a 100 % branch to the 1^+ level at E_x = 0.459 keV with E_γ = 2534 keV. The total number of ^{38}Ca ions collected during the experiment was 1.5×10^8. In Fig. 9, we present a partial view of the γ spectrum in the region of interest. No peak can be observed at 2534 keV. A limit for the $0^+ \rightarrow 0^-$ branch to the level at E_x = 2993 keV has been obtained at the 2σ level (95 % confidence): $I_\beta < 0.0046$ %. This limit is nearly one order of magnitude below the theoretical prediction (I_β = 0.03 %) of Warburton et al. [11].

4 DISCUSSION

4.1 Shell-model description of ^{50}K and ^{38}Ca beta decays

The beta decay of ^{50}K has been previously interpreted by E.K. Warburton [13] with the description of first-forbidden transition as the main motivation. In these shell-model calculations, the WBMB (Warburton-Becker-Millener-Brown) interaction [11, 34] has been used. The WBMB model space consists of the the full *sd* shell ($d_{5/2}, d_{3/2}, s_{1/2}$) together with the full *fp* shell ($f_{7/2}, f_{5/2}, p_{3/2}, p_{1/2}$). The WBMB hamiltonian [34] consists of three parts, the Wildenthal (USD) interaction within the *sd* shell [35], the McGrory interaction within the *fp* shell [36] and the Millener-Kurath potential [11, 37] for the $sd - pf$ cross-shell interaction. Although the WBMB interaction is designed for the full *fp* shell, the original ^{50}K calculations of Warburton had to be truncated because of the large dimension for the 0^- state. For the ^{50}K beta decay we have updated the Warburton calculation by using the full *fp* shell and by using the more recent FPD6 interaction within the *fp* shell [29]. The results of this new calculation will be discussed in Section 4.2.1. The low-lying natural parity states in ^{50}Ca obtained with the FPD6 interaction are in good agreement with the present data (see Fig. 7).

The beta decay of ^{38}Ca, as observed in previous experiments and in this work, proceeds entirely with allowed Gamow-Teller transitions to levels which can be successfully accounted for in the (sd) model space. This result is discussed in Ref.[16]. The evaluation of the first-forbidden transitions which was made previously by Warburton et al. [11] and leads to an overestimation of the $0^+ \rightarrow 0^-$ branch, uses the WBMB interaction. In the last section, the importance of the choice of the cross-shell interaction is discussed.

4.2 Meson-exchange enhancement in ^{50}K and ^{38}Ca decays

4.2.1 ^{50}K(0^-) g.s. $\rightarrow$ ^{50}Ca(0^+) g.s. decay

The experimental matrix element is expressed [11] as:

$$B_1^0 = \left[M_1^0\right]^2 = \frac{6166}{f_0 t}\lambda\!\!\!^{-2}_{ce} \text{ fm}^2 \qquad (6)$$

with t the partial half-life of the transition, f_0 the phase-space factor and $\lambda\!\!\!^{-}_{ce}$ the electron Compton wave length ($\lambda\!\!\!^{-}_{ce}$= 386.159 fm).

For the first-forbidden β_0 branch in the ^{50}K decay, we have

$$I_{\beta_0} = 0.61,\ t = 0.472/0.61$$

and

$$\log f_0 t = 5.89(6)$$

the experimental matrix element is then 34.0 fm. The calculated matrix element is given by equation (2) where $\epsilon_{\rm MEC}$ the enhancement factor over the impulse approximation is obtained from the comparison of the equations (1) and (2) using the values given by Warburton: $a_s\ (Z, W_0, r) = 13.80$, M_0^T (time-like component) = 47.7 and M_0^S (space-like component) = - 2.77. The deduced value is $\epsilon_{\rm MEC} = 1.52(5)$.

Since the original Warburton calculation some progress has been made. It is now possible to calculate the 0^- wave function without the fp shell truncation which was used by Warburton. In addition, the new FPD6 empirical interaction has been developed for the fp shell [29]. The new result for the one-body transition densities are $D_o(5/2) = 0.060$, $D_o(3/2) = 1.354$ and $D_o(1/2) = 0.211$. They do not differ very much from the original Warburton result of $D_o(5/2) = 0.042$, $D_o(3/2) = 1.395$ and $D_o(1/2) = 0.172$. These are then combined with the $M_o(j, \mathrm{eff})$ matrix elements given in Table III of Ref. [13], which contain the core-polarization corrections. The new results are $M_0^T = 41.9$ and $M_0^S = -2.46$, which when compared to experiment gives $\epsilon_{\rm MEC} = 1.62(5)$. This value is in excellent agreement with the value $\epsilon_{\rm MEC} = 1.61$, calculated by Towner [3] in a meson-exchange model. (Pion-exchange processes are computed from a chiral-symmetric phenomenological lagrangian and compared with results obtained in the soft pion approximation).

4.2.2 ^{38}Ca(0^+) g.s.$\rightarrow$ ^{38}K(0^-, E_x = 2993 keV)

The population of the 0^- level in ^{38}K by a beta branch from ^{38}Ca, 0^+, has been evaluated by Warburton et al. [11] to be $I_\beta = 0.03$ %, assuming the current value of $\epsilon_{\rm MEC} = 1.64$ which was the best estimate for light nuclei. The upper limit deduced from our experiment ($I_\beta < 0.0046$ %) clearly disagrees with this first calculation and a different theoretical description is necessary for the understanding of this first-forbidden decay.

The ^{38}Ca 0^+,T=1 $\rightarrow$ ^{38}K 0^-,T=0 transition is discussed in some detail in Ref. [11], because it is one of the few $0^+ \rightarrow 0^-$ transitions which might be experimentally studied in beta decay in the A=40 mass region and because its first-forbidden matrix element was predicted to be unusually large. The other two cases previously mentioned and treated in Ref [11] are the ^{38}S 0^+, T=3 $\rightarrow$ ^{38}Cl 0^-, T=2 and the ^{44}Ti 0^+,T=0 $\rightarrow$ ^{44}Sc, 0^-, T=1 transitions (see Table VI of Ref. [11]). Here we will discuss the interpretation of the ^{38}Ca and ^{38}S decays.

The allowed configurations in the notation of sd-shell holes and fp-shell particles are: ^{38}Ca 0^+,T=1 $[(sd)^{-2}]$ $(0\hbar\omega)$; ^{38}K 0^-,T=0 $[(sd)^{-3} \times (fp)]$ $(1\hbar\omega)$; ^{38}S 0^+,T=3 $[(sd)^{-4} \times (fp)^2]$ $(0\hbar\omega)$ and ^{38}Cl 0^-,T=2 $[(sd)^{-3} \times (fp)]$ $(1\hbar\omega)$ with all possible couplings of the intermediate angular momentum. The discussion below will be based upon equation (2) with the value $\epsilon_{\rm MEC}$=1.64 as used in Ref. [11] which is consistent with the present analysis of the ^{50}K decay. The kinematical factors a_s are -2.31 and 4.96 for ^{38}Ca and ^{38}S, respectively. The theoretical M_0 values implicitly include the factors $q_T = 0.9$ and $q_S = 1.1$ (see Sec. C of Ref. [11]), which approximately take into account the truncation of the many $\hbar\omega$ space to $0\hbar\omega$ and $1\hbar\omega$ (the core-polarization corrections) and the use of the harmonic-oscillator radial wave functions (rather than the more realistic Woods-Saxon form). The experimental values are $M_1^0(\mathrm{expt}) = 11.8 \pm 0.6$ for ^{38}S (Table VI of Ref. [11]) and a limit of $M_1^0(\mathrm{expt}) \leq 20$ from the present limit of the branching ratio.

As discussed in Sec. H of Ref. [11] there are several complications with the ^{38}K, 0^- state. The 0^- state is predicted to be 1470 keV higher than observed. Also, the 0^- state has two large components, (a) $(sd)^{-3}[J = 3/2^+, T = 1/2, n = 1] \times (p_{3/2})$ and (b) $(sd)^{-3}[J = 7/2^+, T = 1/2, n = 1] \times (f_{7/2})$, where $(sd)^{-3}[J = 3/2^+, T = 1/2, n = 1]$ and $(sd)^{-3}[J = 7/2^+, T = 1/2, n = 1]$ are the wave functions for the first $3/2^+$ and $7/2^+$ states of ^{37}K (or ^{37}Ar). For the WBMB interaction the probabilities of (a) and (b) in the lowest 0^- state are both large, $P_a = 41$ % and $P_b = 37$ %, respectively. There is another 0^- state 600 keV higher in energy which has roughly the "orthogonal" configuration with P_a=48 % and P_b=44 %. These two configurations are both important because the $(sd)^{-3}[J = 7/2^+, n = 1]$ state lies 2.2 MeV higher than the $(sd)^{-3}[J = 3/2^+, n = 1]$ state in A=37 while the $p_{3/2}$ single-particle state lies 1.9 MeV higher than the $f_{7/2}$ in A=41. The ^{38}Ca 0^+,T=1 $(sd)^{-2}$ state is relative simple, with 94 % being in the $(d_{3/2})^{-2}$ configuration. The dominant term in the first-forbidden transition is $d_{3/2} \rightarrow p_{3/2}$ which can only connect

the ^{38}Ca initial state with component (a) in ^{38}K. Thus, the first-forbidden strength is approximately equally divided between the first ($M_1^0 = 55$) and second ($M_1^0 = 57$) 0^- final states.

The division of strength between these two 0^- states might be sensitive to the hamiltonian and we must assume that the WBMB hamiltonian is not quite correct since the energy of the 0^- state is predicted 1470 keV too high. In order to test this we have used another cross-shell interaction proposed by Warburton [38]. It differs from the Millener-Kurath part of the WBMB hamiltonian mainly in a 20 % increase in the overall strength which was chosen in order to better reproduce the energies of $1\hbar\omega$ particle-hole states in ^{40}Ca. The lowest 0^- state in ^{38}K is still too high (by 1100 keV), however the wave functions of the lowest two 0^- states and the resulting matrix elements change dramatically (see **Table VI**); for the first state, P_a=9 %, P_b=62 %, $M_1^0 = 24$, and for the second state. P_a=76 %, P_b=12 %, $M_1^0 = 63$. The new result is marginally consistent with M_1^0(expt) ≤ 20 (for the first 0^- state) from the present experiment. But more importantly this shows the sensitivity of the ^{38}Ca decay to the cross-shell hamiltonian. The theoretical matrix element will not be known with confidence until the energies are better reproduced. The ^{38}Ca decay experiment can be interpreted in terms of providing a limit on the size of the (a) ($p_{3/2}$ single-particle) component in the 0^- wave function.

In contrast to the ^{38}K, 0^- state, the wave function for the ^{38}Cl, 0^- state is more stable and is dominated by the $(sd)^{-3}[J = 3/2^+, T = 3/2, n = 1] \times (p_{3/2})$ component. The reason for this is that there is no low-lying J=$7/2^+$ state in ^{37}Cl as there was above in ^{37}K. The WBMB interaction gives $M_1^0 = 19.0$ and the modified particle-hole interaction gives $M_1^0 = 12.3$. The latter is in excellent agreement with the experimental value of M_1^0(expt) $= 11.8 \pm 0.6$.

5 Summary and Conclusion

Two $\Delta J = 0$, first-forbidden transitions have been studied in detail as, for both, a large mesonic enhancement was predicted for the matrix element M_0^T of the time-like component of the weak-axial current. The strong ^{50}K, 0^- g.s. $\rightarrow^{50}$Ca, 0^+ g.s. decay has been established from a detailed account of the observed activity. For this transition (mostly $p_{3/2} \rightarrow d_{3/2}$), the enhancement factor, $\epsilon_{\rm MEC} = 1.62(5)$, by which M_0^T exceeds the impulse approximation value, is right in line of similar values previously reported for $s_{1/2} \leftrightarrow p_{1/2}$ transitions in light nuclei. The excellent agreement with predicted values illustrates the validity of the FPD6 interaction which is also demonstrated by the description of the ^{50}Ca bound states observed in our experiment.

On the other hand, the predicted enhancement could not be confirmed for the ^{38}Ca, 0^+ g.s. $\rightarrow^{38}$K, 0^-(E$_x$ = 2.993 MeV) decay despite unprecedented experimental conditions. The theoretical prediction can be found in better agreement with the experimental result with another choice for the cross-shell interaction, but it remains difficult to reproduce the excitation energy of the ^{38}K 0^- state and consequently to describe the different components of this state.

For this mass region, the ^{50}K first-forbidden beta decay provides the best case for interpreting the effects of meson-exchange enhancement. The reason is that the $p_{3/2}$ neutron and the $d_{3/2}$ proton states are both at the Fermi surface in ^{50}K with the result that the wave functions for ^{50}K and ^{50}Ca are rather simple and dominated by components which give a large first-forbidden matrix element. In contrast, for the region around ^{40}Ca the $p_{3/2}$ is an excited state relative to $f_{7/2}$. The resulting configurations which lead to large first-forbidden matrix elements are thus at a higher excitation and their mixture into the states observable in beta decay are more sensitive to the hamiltonian as we have shown in the case of the ^{38}K, 0^- state.

Acknowledgements :

We are indebted to the late E.K. Warburton for his seminal work which instigated this experiment. We wish to thank the ISOLDE Technical Group for the target/ion source developments allowing pure Ca beams. This work was supported by IN2P3 (Institut National de Physique Nucléaire et de Physique des Particules). B.A. Brown would like to acknowledge support from the Alexander van Humboldt Foundation and from NSF grant 9605207.

References

[1] K. Kubodera, J. Delorme, and M. Rho, Phys. Rev. Lett. **40**, 755 (1978).

[2] P. Guichon, M. Giffon, J. Joseph, R. Laverrière, and C. Samour, Z. Phys. A **285**, 183 (1978); P. Guichon, M. Giffon, and C. Samour, Phys. Lett. **74B**, 15 (1978).

[3] I.S. Towner, Comments Nucl. Part. Phys. **15**, 145 (1986).

[4] M. Kirchbach and M. Reinhardt, Phys. Lett. **208**, 2 (1988).

[5] E.K. Warburton, in Interactions and Structures in Nuclei, edited by R. Blin-Stoyle and W. Hamilton (Adam Hilger, Bristol, England, 1988), pp.81-88.

[6] E.K. Warburton, I.S. Towner, and B.A. Brown, Phys. Rev. C **49**, 824 (1994).

[7] H. Mach, E.K. Warburton, R.L. Gill, R.F. Casten, J.A. Becker, B.A. Brown, and J.A. Winger, Phys. Rev. C **41**, 226 (1990).

[8] E.K. Warburton, Phys. Rev. Lett. **66**, 1823 (1991) and Phys. Rev. C **44**, 233 (1991).

[9] I.S. Towner, Nucl. Phys. **A542**, 631 (1992).

[10] M. Rho, Phys. Rev. Lett. **66**, 1275 (1991).

[11] E.K. Warburton, J.A. Becker, B.A. Brown, and D.J. Millener, Ann. Phys. (N.Y.) **187**, 471 (1988).

[12] G. Walter, P. Baumann, M. Bounajma, Ph. Dessagne, A. Huck, G. Klotz, A. Knipper, Ch. Miehé, J. Rachidi, M. Ramdhane, G. Marguier, C. Richard-Serre, A. Dobado, and A. Poves, in Proceedings on Nuclear Structure of Light Nuclei far from Stability : Experiment and Theory, Obernai (France), November 27-29, p.71 (1989).

[13] E.K. Warburton, Phys. Rev. C **44**, 1024 (1991).

[14] T.W. Burrows, Nucl. Data Sheets **75**, 1 (1995).

[15] H.S. Wilson, R.W. Kavanagh, and F.M. Mann, Phys. Rev. C **22**, 1696 (1980).

[16] B.D. Anderson, A.R. Baldwin, P. Baumann, B.A. Brown, F. Didierjean, C.C. Foster, L.A.C. Garcia, A. Huck, A. Knipper, R. Madey, D.M. Manley, G. Marguier, M. Ramdhane, H. Ravn, C. Richard-Serre, G. Walter, and J.W. Watson, Phys. Rev. C **54**, 602 (1996).

[17] E. Hagebö, P. Hoff, O.C. Jonsson, E. Kugler, J.P. Omtvedt, H.L. Ravn, and K. Steffensen, Nucl. Instr. Methods Phys. Res. B **70**, 165 (1992).

[18] P.M. Endt, Nucl. Phys. **A521**, 1 (1990).

[19] M. Bounajma, Thèse, Université de Strasbourg (1996).

[20] N.W. Hill, J.A. Harvey, D.J. Horen, G.L. Morgan, and R.R. Winters, IEEE Trans. Nucl. Sc. NS **32**, 367 (1985).

[21] A. Huck, G. Klotz, A. Knipper, Ch. Miehé, C. Richard-Serre, G. Walter, A. Poves, H.L. Ravn, and G. Marguier, Phys. Rev. C **31**, 2226 (1985).

[22] Ch. Miehé, Ph. Dessagne, P. Baumann, A. Huck, G. Klotz, A. Knipper, G. Walter, and C. Richard-Serre, Phys. Rev. C **33**, 1736 (1986).

[23] L.C. Carraz, P.G. Hansen, A. Huck, B. Johnson, G. Klotz, A. Knipper, K.L. Kratz, Ch. Miehé, S. Mattson, G. Nymann, H. Ohm, A.M. Poskanser, A. Poves, H.L. Ravn, C. Richard-Serre, A. Schröder, G. Walter, and W. Ziegert, Phys. Lett. **109B**, 419 (1982).

[24] M. Langevin, C. Détraz, D. Guillemaud-Mueller, A.C. Mueller, C. Thibault, F. Touchard, G. Klotz, C. Miehé, G. Walter, M. Epherre, and C. Richard-Serre, Phys. Lett. **130B**, 251 (1983).

[25] W. Ziegert, Diplomarbeit, Mainz (1980).

[26] J. Rachidi, Thèse, Université de Strasbourg (1983).

[27] T.W. Burrows, Nucl. Data Sheets **76**, 191 (1995).

[28] C. Détraz, D. Guillemaud, G. Huber, R. Klapisch, M. Langevin, F. Naulin, C. Thibault, L.C. Carraz, and F. Touchard, Nucl. Phys. **A302**, 41 (1978).

[29] W.A. Richter, M.G. Van der Merwe, R. E. Julies, and B.A. Brown, Nucl. Phys. **A523**, 325 (1991).

[30] D.G. Sandler, S.E. Koonin, and W.A. Fowler, Astrophys. J. **259**, 908 (1982).

[31] K.L. Kratz (private communication).

[32] P.M. Endt, At. Data Nucl. Data Tables **55**, 171 (1993).

[33] D.G. Rickel, M.R. Roberson, J.D. Turner, H.R. Weller, and D.R. Tilley, Phys. Rev. C **13**, 2077 (1976).

[34] E.K. Warburton and J.A. Becker, Phys. Rev. C **37**, 754 (1988) ; J.A. Becker, E. K. Warburton, and B.A. Brown, Phys. Rev. C **41**, 1147 (1990).

[35] B.A. Brown and B.H. Wildenthal, Ann. Rev. Nucl. Part. Sci. **38**, 29 (1988).

[36] J.B. McGrory, Phys. Rev. C **8**, 693 (1973).

[37] D.J. Millener and D.Kurath, Nucl. Phys. **A255**, 315 (1975).

[38] E.K. Warburton, Brookhaven National Laboratory Report 40890 (1987).

Figure Captions

Figure 1 : Diagram of the ^{50}K decay modes illustrating the different daughter activities of a pure ^{50}K source.

Figure 2 : Beta decay curve of ^{26}Na. The inset shows a schematic ^{26}Na decay scheme. The fitted half-life ($T_{1/2} = 1.066 \pm 0.002$) is more precise than the adopted one ($T_{1/2} = 1.072 \pm 0.009$, Ref. 18).

Figure 3 : Left, setup for the low energy neutron detection : NE102A plastic counters at 75 cm from the collection point associated with a Ge detector. At the center, the collection point is surrounded by a thin cylindrical plastic scintillator.
Right, schematic view of one counter for low energy neutron detection.

Figure 4 : Beta emission at mass A = 50 (curve 1). The best fit between the experimental and calculated decay curves is obtained with the sum of the different components : curve 2 (^{50}K decay and daughters), curve 3 (^{50}Ca decay and daughters), curve 4 (^{50m}Sc decay), curve 5 (^{50}Sc decay and a constant background).

Figure 5 : Partial view of the $\beta - \gamma$ spectrum gated by the 1027 γ line. The γ energies are labelled in keV.

Figure 6 : Neutron time-of-flight spectrum related to the ^{50}K decay resulting from a mixing of the stop signals given by the 12 plastic counters, the start signal being given by the β counter. The neutron energies are labelled in MeV.

Figure 7 : Disintegration scheme of ^{50}K. The ^{50}Ca positive parity states are compared to shell-model calculations with the FPD6 interaction. Results of the calculations are reported in the frame.

Figure 8 : Experimental B(GT) distribution in the ^{50}K decay represented by summing the strength within 500 keV intervals. We reported B(GT) values (Table III) corresponding to transitions with log $ft < 5.8$.

Figure 9 : Left: partial view of the $\beta - \gamma$ spectrum related to the ^{38}Ca decay. We note the absence of the 2534 keV γ line. Right: as a comparison, we represent the line at $E_\gamma = 1.57$ MeV ($1^+ \rightarrow 0^+$, ^{38}K) from the ^{38}Ca β decay, registered during the same time.

Table Captions

TABLE I : Energy, intensity and assignment of the γ transitions in ^{50}Ca populated by the ^{50}K β decay

TABLE II : Energy levels and the γ-ray branching ratios in ^{50}K β decay

TABLE III : Excitation energy (in keV) of ^{50}Ca levels populated in the β decay of ^{50}K, beta intensities and the corresponding log ft values. B(GT) values are also reported for $E_x > 6$ MeV where allowed transitions are expected. Values in parenthesis correspond to transitions with high log ft values for which the allowed character is not established

TABLE IV : Energy, intensity and proposed assignment for the β-delayed neutrons in the ^{50}K β decay

TABLE V : Energy, intensity and assignment of the γ transitions in ^{49}Ca populated in the ^{50}K β decay

TABLE VI : Excitation energy of the first two 0^- levels and amplitude of the bare matrix elements of the corresponding $0^+ \rightarrow 0^-$ transitions calculated with different interactions. For the ^{38}Ca to ^{38}K decay, a_s = -2.31 and for ^{38}S to ^{38}Cl, a_s = 4.96

TABLE I

E_γ (keV)	I_γ (relative)	Transition (keV)
1027.0 (5)	100	1027 - 0
1975.3 (5)	12.9 (1.0)	3002 - 1027
2504.9 (5)	6.4 (0.8)	3532 - 1027
3008.9 (5)	20.2 (1.3)	4036 - 1027
3449.0 (5)	2.9 (0.8)	4476 - 1027
3531.8 (5)	5.9 (0.8)	3532 - 0
4035.6 (5)	33.5 (2.0)	4036 - 0
4886.0 (5)	16.6 (1.4)	4886 - 0

TABLE II

E_i (keV)	E_f (keV)	Gamma branching ratio (%)
1027.0 (5)	0	100
3002.3 (7)	1027.0	100
3531.9 (4)	1027.0	52 (4)
	0	48 (4)
4035.8 (4)	1027.0	38 (2)
	0	62 (2)
4476.0 (7)	1027.0	100
4886.2 (5)	0	100

TABLE III

E_x (keV)	I_β (%)	log ft	B(GT) x 10^{+2}
0	61.0 (7.4)	5.89 ± 0.06	
1027.0 (5)	3.69 (41)	6.95 ± 0.06	
3002.3 (7)	0.83 (14)	7.27 ± 0.09	
3531.9 (4)	0.79 (14)	$7.20^{+0.09}_{-0.10}$	
4035.8 (4)	3.45 (53)	$6.46^{+0.07}_{-0.08}$	
4476.0 (7)	0.19 (6)	$7.62^{+0.13}_{-0.17}$	
4886.2 (5)	1.06 (18)	$6.82^{+0.08}_{-0.11}$	
6508 (12)	1.28 (47)	$6.34^{+0.16}_{-0.24}$	(0.3)
7026 (36)	0.38 (8)	$6.71^{+0.11}_{-0.13}$	(0.1)
7261 (46)	0.29 (8)	$6.76^{+0.13}_{-0.16}$	(0.1)
7303 (50)	0.38 (15)	$6.63^{+0.16}_{-0.23}$	(0.2)
7613 (65)	1.74 (92)	$5.88^{+0.20}_{-0.34}$	(0.8)
7992 (85)	0.75 (31)	$6.11^{+0.18}_{-0.24}$	(0.5)
8236 (95)	0.81 (38)	$6.02^{+0.19}_{-0.29}$	(0.6)
8798 (120)	9.83 (1.81)	$4.73^{+0.12}_{-0.15}$	11.5
9235 (130)	5.57 (1.13)	$4.82^{+0.14}_{-0.16}$	9.3
9766 (140)	2.55 (1.01)	$4.93^{+0.19}_{-0.26}$	7.2
10430 (150)	0.93 (20)	$5.05^{+0.17}_{-0.19}$	5.5
10540 (160)	2.49 (94)	$4.57^{+0.21}_{-0.27}$	16.6
11050 (170)	0.90 (21)	$4.73^{+0.21}_{-0.23}$	11.5
11470 (170)	1.05 (25)	$4.38^{+0.24}_{-0.25}$	25.7

TABLE IV

E_n (keV)	I_n (relative)	$E_x(^{50}Ca)$ - $E_f(^{49}Ca)$
152(8)	17(6)	6510 - 0
446(25)	4(1)	10430 - 3585
497(25)	31(13)	8800 - 2023
642(35)	4(1)	11050 - 4072
660(35)	5(1)	7030 - 0
689(35)	7(2)	10430 - 3358
844(45)	8(3)	9230 - 2023
890(45)	4(1)	7260 - 0
931(50)	5(2)	7300 - 0
986(50)	5(2)	11470 - 4072
1102(60)	6(2)	11050 - 3585
1235(65)	23(12)	7610 - 0
1362(70)	5(2)	9770 - 2023
1606(85)	10(4)	7990 - 0
1741(90)	7(2)	11470 - 3358
1845(95)	11(5)	8240 - 0
2012(105)	25(12)	10540 - 2023
2396(120)	100(15)	8800 - 0
2824(130)	66(13)	9230 - 0
3345(140)	29(13)	9770 - 0
3980(150)	2(1)	10430 - 0
4010(160)	8(2)	10540 - 0
4600(170)	2(1)	11050 - 0
5010(170)	2(1)	11470 - 0

TABLE V

E_γ (keV)	I_γ (relative)	Transition (keV)
2023.0 (5)	100	2023.0 - 0
3356.7 (1.0)	5.6 (1.2)	3356.8 - 0
3586.0 (5)	4.2 (1.5)	3586.1 - 0
3859.7 (9)	7.9 (1.3)	3859.9 - 0
4072.0 (1.0)	7.3 (2.0)	4072.2 - 0

TABLE VI

	Interaction	J,n	E_x (MeV)	M_0^T	M_0^S	M_1^0
^{38}K	WBMB	0^-(1)	4.46	34.7	1.98	52
		(2)	5.07	35.8	2.05	54
	WBMB (mod)	0^-(1)	4.08	16.1	0.91	24
		(2)	5.39	41.8	2.39	63
^{38}Cl	WBMB	0^-(1)	1.74	14.0	- 0.79	19.0
		(2)	5.19	2.9	- 0.16	3.9
	WBMB (mod)	0^-(1)	1.78	9.0	- 0.51	12.3
		(2)	4.39	2.9	- 0.16	3.9

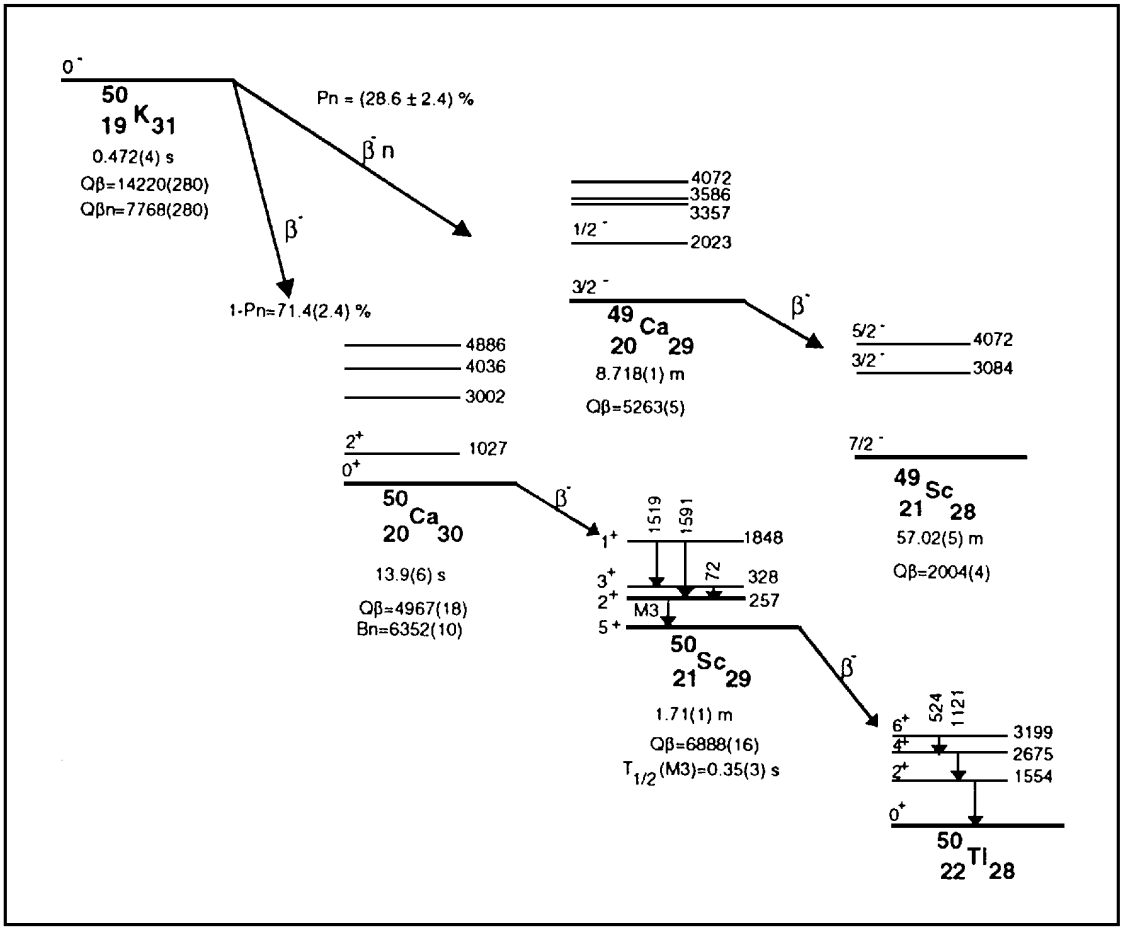
0-
50 19 K 31
0.472(4) s
Qβ=14220(280)
Qβn=7768(280)
Pn = (28.6 ± 2.4) %
β- n
β-
1-Pn=71.4(2.4) %
4886
4036
3002
2+ 1027
0+
50 20 Ca 30
13.9(6) s
Qβ=4967(18)
Bn=6352(10)
4072
3586
3357
1/2- 2023
3/2-
49 20 Ca 29
8.718(1) m
Qβ=5263(5)
β-
1519
1591
1+ 1848
72
3+ 328
2+ 257
M3
5+
50 21 Sc 29
1.71(1) m
Qβ=6888(16)
T1/2(M3)=0.35(3) s
β-
5/2- 4072
3/2- 3084
7/2-
49 21 Sc 28
57.02(5) m
Qβ=2004(4)
524
1121
6+ 3199
4+ 2675
2+ 1554
0+
50 22 Ti 28

Fig. 1

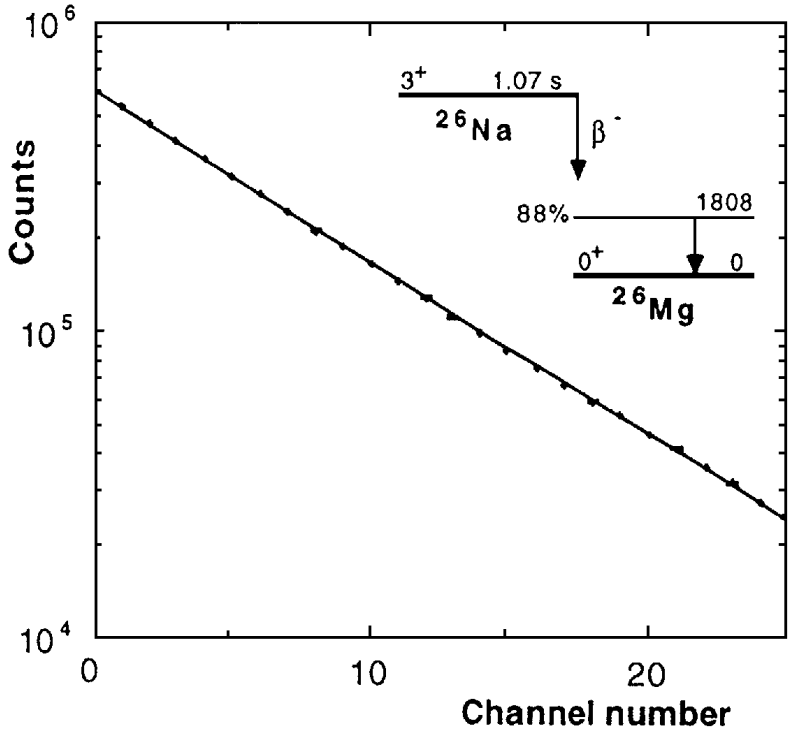
10^6
10^5
10^4
Counts
0
10
20
Channel number
3+
1.07 s
26Na
β-
88%
1808
0+
0
26Mg

Fig. 2

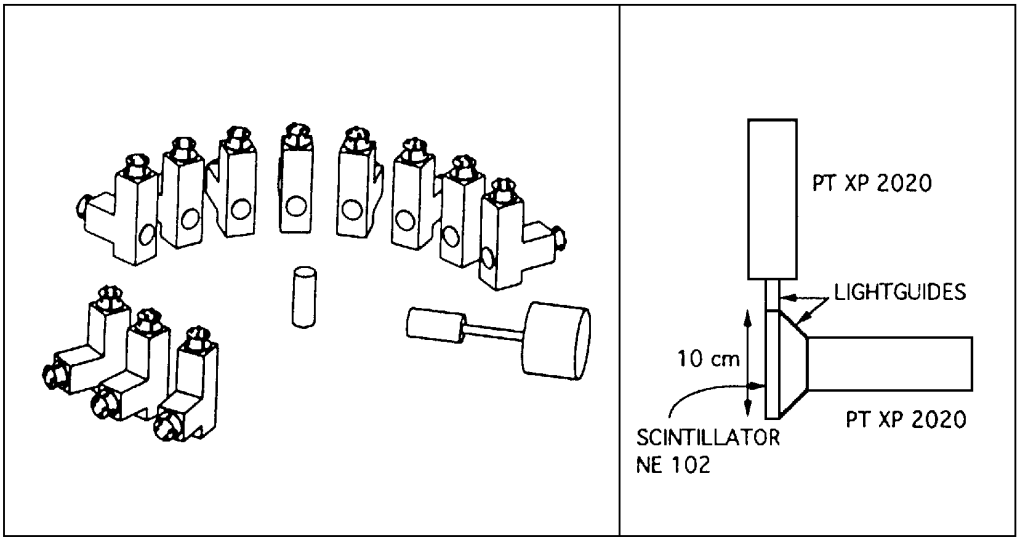
PT XP 2020
LIGHTGUIDES
10 cm
PT XP 2020
SCINTILLATOR
NE 102

Fig. 3

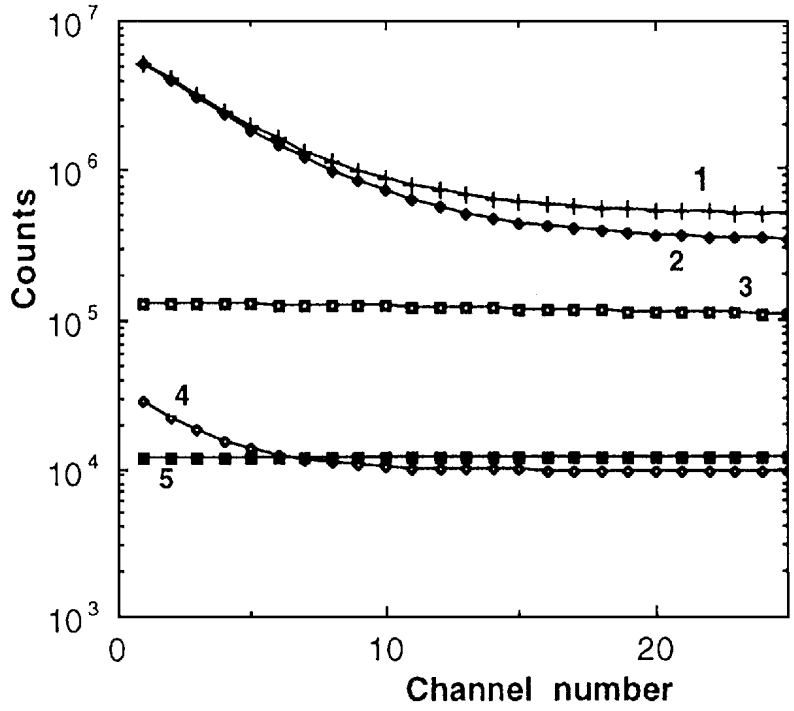
Counts
Channel number
1
2
3
4
5

Fig. 4

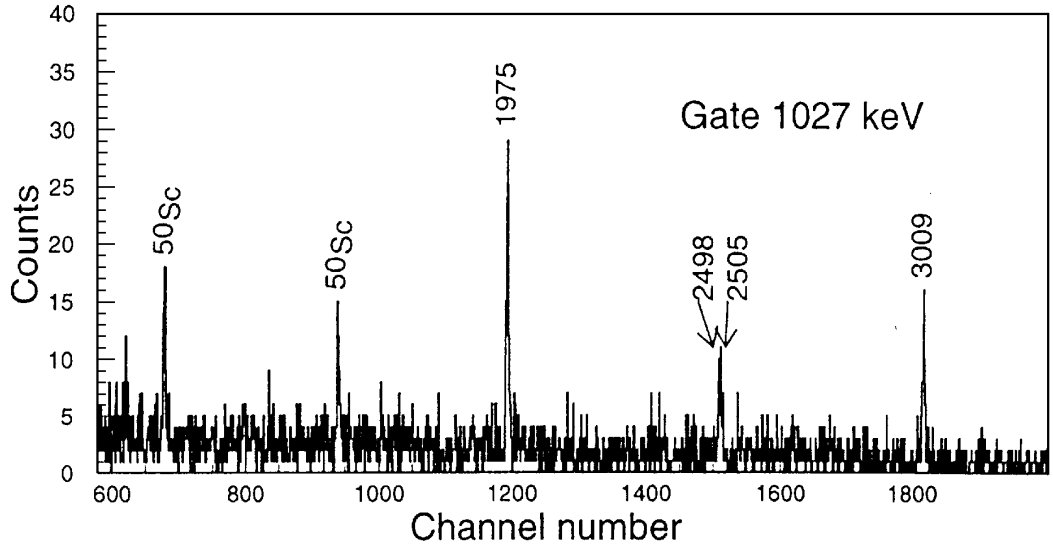
Counts
Channel number
Gate 1027 keV
50Sc
50Sc
1975
2498
2505
3009

Fig. 5

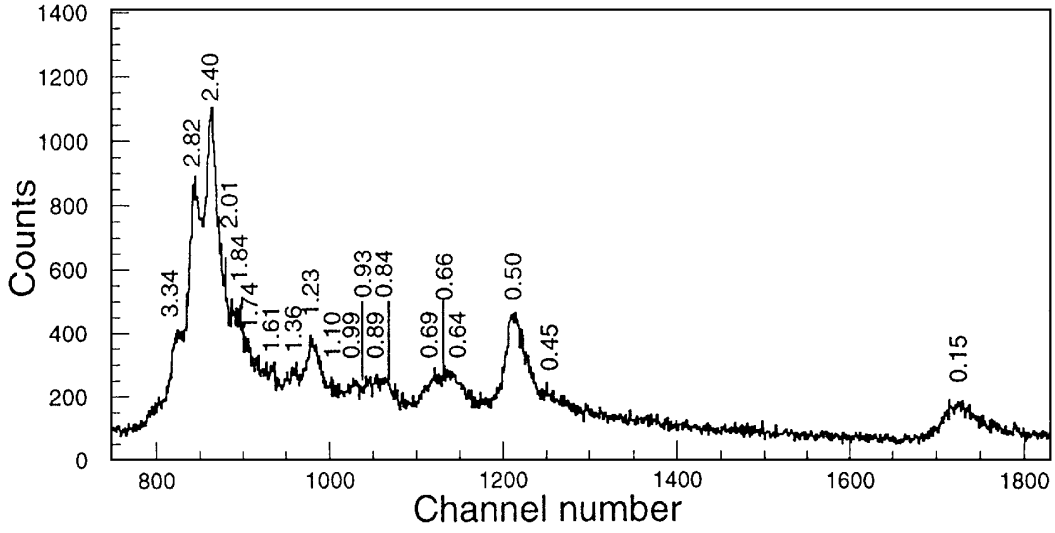
Counts
Channel number
0
200
400
600
800
1000
1200
1400
800
1000
1200
1400
1600
1800
3.34
2.82
2.40
2.01
1.84
1.74
1.61
1.36
1.23
1.10
0.99
0.93
0.89
0.84
0.69
0.66
0.64
0.50
0.45
0.15

Fig. 6

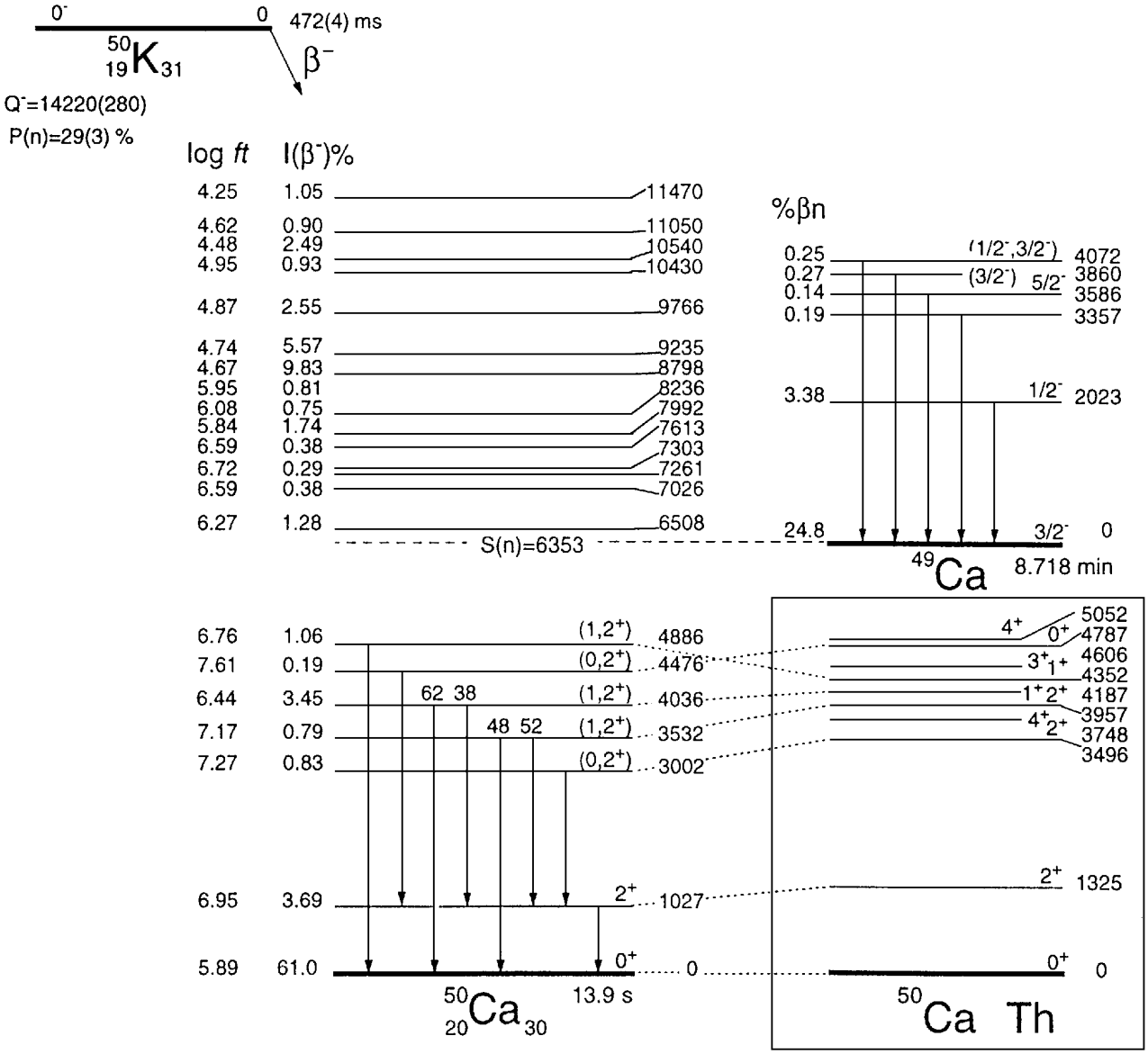
0⁻
0
472(4) ms
50 19K31
β⁻
Q⁻=14220(280)
P(n)=29(3) %
log ft
I(β⁻)%
4.25 1.05 11470
4.62 0.90 11050
4.48 2.49 10540
4.95 0.93 10430
4.87 2.55 9766
4.74 5.57 9235
4.67 9.83 8798
5.95 0.81 8236
6.08 0.75 7992
5.84 1.74 7613
6.59 0.38 7303
6.72 0.29 7261
6.59 0.38 7026
6.27 1.28 6508
S(n)=6353
%βn
0.25 (1/2⁻,3/2⁻) 4072
0.27 (3/2⁻) 5/2⁻ 3860
0.14 3586
0.19 3357
3.38 1/2⁻ 2023
24.8 3/2⁻ 0
49Ca
8.718 min
6.76 1.06 (1,2⁺) 4886
7.61 0.19 (0,2⁺) 4476
6.44 3.45 (1,2⁺) 4036
62 38
7.17 0.79 (1,2⁺) 3532
48 52
7.27 0.83 (0,2⁺) 3002
6.95 3.69 2⁺ 1027
5.89 61.0 0⁺ 0
50 20Ca30
13.9 s
4⁺ 0⁺ 5052 4787
3⁺1⁺ 4606 4352
1⁺2⁺ 4187
4⁺2⁺ 3957 3748 3496
2⁺ 1325
0⁺ 0
50Ca Th

Fig. 7

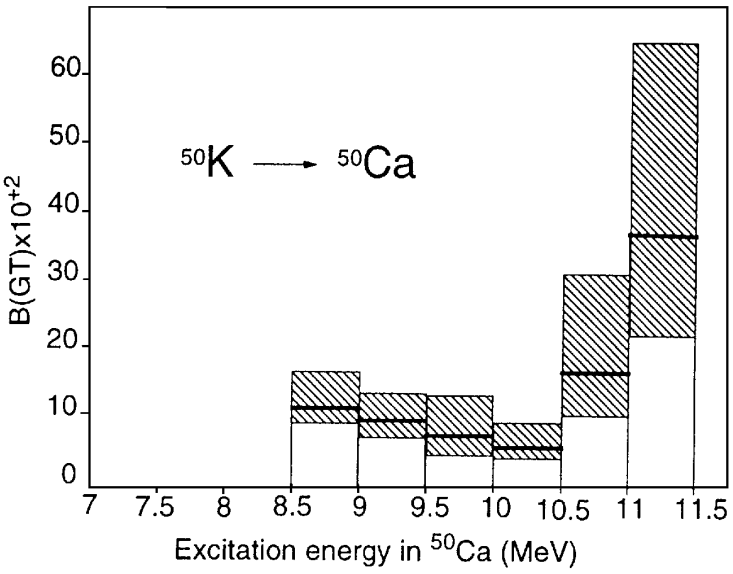
$^{50}K \longrightarrow {}^{50}Ca$
B(GT)x10^{+2}
60
50
40
30
20
10
0
7
7.5
8
8.5
9
9.5
10
10.5
11
11.5
Excitation energy in ^{50}Ca (MeV)

Fig. 8

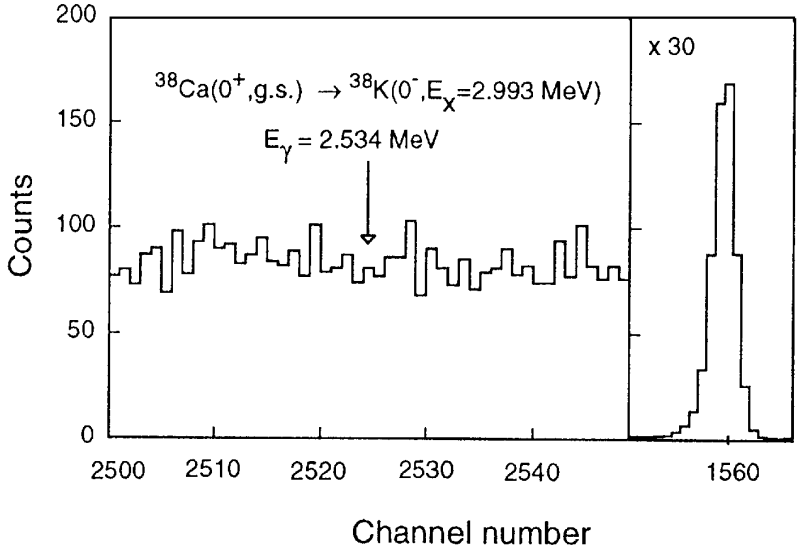
$^{38}Ca(0^+,g.s.) \rightarrow {}^{38}K(0^-,E_x=2.993\ MeV)$
$E_\gamma = 2.534$ MeV
x 30
Counts
200
150
100
50
0
2500
2510
2520
2530
2540
1560
Channel number

Fig. 9